Enhancing Ultimate Bearing Capacity Assessment of Rock Foundations using a Hybrid Decision Tree Approach

Mei Guo, Ren-an Jiang
College of Road and Bridge Engineering, Jilin Communications Polytechnic, Changchun Jilin, 130012, China

***Abstract*—Accurately estimating the ultimate bearing capacity of piles embedded in rock is of paramount importance in the domains of civil engineering, construction, and foundation design. This research introduces an innovative solution to tackle this issue, leveraging a fusion of the Decision Tree method with two state-of-the-art optimization algorithms: the Zebra Optimization Algorithm and the Coronavirus Herd Immunity Optimizer. The research approach encompassed the creation of a hybridized model, unifying the DT with the Zebra Optimization Algorithm and Coronavirus Herd Immunity Optimizer. The primary objective was to augment the precision of the ultimate bearing capacity of prediction for piles embedded in rock. This hybridization strategy harnessed the capabilities of DT along with the two pioneering optimizers to address the inherent uncertainty stemming from diverse factors impacting bearing capacity. The Zebra Optimization Algorithm and Coronavirus Herd Immunity Optimizer showcased their efficacy in refining the base model, leading to substantial enhancements in predictive performance. This study's discoveries make a significant stride in the realm of geotechnical engineering by furnishing a sturdy approach to forecasting ultimate bearing capacity in rock-socketed piles. The hybridization method is a hopeful path for future research endeavors and practical implementations. Specifically, the DT + Zebra Optimization Algorithm model yielded dependable outcomes, as evidenced by their impressive R-squared value of 0.9981 and a low Root mean squared error value of 629.78. The attained outcomes empower engineers and designers to make well-informed choices concerning structural foundations in soft soil settings. Ultimately, this research advocates for safer and more efficient construction methodologies, mitigating the hazards linked to foundation failures.**

Keywords*—Ultimate bearing capacity; decision tree; zebra optimization algorithm; coronavirus herd immunity optimizer

I. Introduction

A. Background

Pile foundations are essential for the structural load transmission into the ground, guaranteeing the stability of the structure. Precisely assessing the load-bearing capacity of piles holds paramount importance in planning geotechnical structures [1]. Numerous experimental and theoretical approaches established in the past for predicting pile capacity rely on assumptions related to the factors governing the ultimate bearing capacity (Q_u) [2]. Nevertheless, owing to the intricate behavior of piles, nearly all of the existing methods and models fall short of delivering precise predictions, and a considerable number of them are tailored to specific construction sites [3].

While the static load test (SLT) remains the most reliable approach for evaluating pile-bearing capacity, its implementation can be a time-consuming, expensive, and demanding process [4]. An advanced method for forecasting the bearing capacity of piles is high-strain dynamic testing ($HSDT$). This method relies on wave propagation theory and is executed by utilizing a pile-driving analyzer (PDA). The HSDT process is usually standardized according to American Standard Test Methods [5]. Previous studies have revealed a strong correlation between the bearing capacity projected through PDA and values anticipated through SLT.

Moreover, PDA (HSDT) offers the advantages of enhanced speed and cost-effectiveness when compared to SLT. However, the attainment of trustworthy results mandates the execution of multiple PDA tests for every construction project. Hence, the aim to reduce the necessary number of PDA tests is of great significance, as it would reduce overall project costs. In pursuit of this goal, novel techniques such as artificial intelligence (AI) have surfaced, demonstrating the ability to provide more accurate forecasts of pile-bearing capacity and expedite solutions for complex engineering problems compared to traditional methods [6].

B. Literature Review

Machine learning (ML) methods have recently become pivotal in civil engineering and geotechnical projects. They streamline labor-intensive engineering procedures and substantially contribute to these projects' cost efficiency. Additionally, numerous research studies utilize ML techniques to estimate the Q_u (ultimate bearing capacity) of rocks [7,8]. Yagiz et al. [9] presented ANN models, whereas Jahed Armaghani et al. [10] introduced adaptive neuro-fuzzy inference system ($ANFIS$) models to forecast rock strength. Concurrently, Singh et al. [11] recorded the effective application of an $ANFIS$ estimation model to estimate the Young's modulus of rock. In another study, Shirani Faradonbeh et al. [12] conducted research focused on developing a genetic programming (GP) technique for predicting backbreak caused by blasting. Monjezi et al. [13] applied ANN models to forecast ground vibration, whereas Marto et al. [14] utilized imperial competitive algorithm (ICA)-ANN models to predict fly rock incidents in their studies. Azimi et al. [15] also proposed a new control method, called Swarm-Based Parallel Control (SPC), inspired by the intelligence of swarms in

nature. In this study, sharing the response data among adjacent buildings using a wireless sensor network (WSN) at each floor is proposed to improve the seismic performance and minimize the risks of knocking.

In foundation design and analysis, these methodologies have garnered extensive usage. For example, Chan et al. [13] introduced an ANN model as a substitute for developing pile-driving formulas. In this scenario, the neural network was trained to employ data associated with the pile configuration, the energy employed during pile driving, and the elastic compression of the pile and the soil, with the ultimate bearing capacity (Q_u) of the pile as the network's output. In a separate investigation by Pal and Deswal [16], they developed two soft computing approaches, namely ANN and support vector machine (SVM), to evaluate the Q_u of concrete spun pipe piles. Their results demonstrated that among the models examined, ANN delivered the highest level of predictive accuracy. Shahin et al. [17] designed an ANN predictive model for foreseeing the bearing capacity of drilled shafts. In a distinct study, Jianbin et al. [18] evidenced the effectiveness of ANN in forcating the axial bearing capacity (ABC) of pipe piles in sandy soil. They included significant factors like the effective length and diameter of the pile, soil cohesion, unit weight, internal friction angle, and results from the standard penetration test (SPT) in the development of the network. In another research endeavor, Yu Lei et al. [19] conducted a comparative study involving six hybrid models that incorporated neural networks in conjunction with six different swarm intelligence optimization algorithms, including the innovative Seagull Optimization Algorithm (SOA). These hybrid models were evaluated against the predictive capabilities of two single models without any optimization techniques in forecasting Uniaxial Compressive Strength. Moreover, other researchers have contributed to the advancement of meta-heuristic algorithms. For instance, Agushaka [20] conducted studies aimed at enhancing arithmetic optimization, while Gaurav Dhiman et al. [21] focused on refining the Seagull Optimization Algorithm. These efforts collectively contribute to developing and improving hybrid models that leverage both ML techniques and advanced optimization methods for enhanced predictive accuracy.

C. Objective

This research introduces a novel ML approach to attain precise and optimal predictions. The hybridization method employed in this study is custom-tailored to enhance the performance of DT models, guaranteeing reliable outcomes. Through the combination of 2 cutting-edge and effective optimization techniques, namely the Zebra Optimization Algorithm (ZOA) and the Coronavirus Herd Immunity Optimizer (CHIO, the creation of these innovative hybrid models exceeded the capabilities of traditional methods, marking a substantial leap forward. A thorough assessment was carried out on these models, individually and in hybrid setups, to guarantee a fair and unbiased evaluation of their performance. To ensure the trustworthiness of the outcomes, the evaluation of model outputs included well-recognized performance metrics such as R^2 and RMSE. This approach played a crucial role in mitigating any possible bias in the results, offering a more precise understanding of the models' effectiveness. In addition to the technical aspects, this study acknowledged the practical importance of these discoveries. The increased precision achieved with the hybrid models holds the promise of improving decision-making in real-world geotechnical engineering projects, thus reducing the risks associated with inaccurate Q_u estimations. The ability of the DT model to provide dependable predictions, whether applied individually or in hybrid configurations, highlights their flexibility and appropriateness for various project needs.

II. Materials and Methodology

A. Data Gathering

In ML projects, the careful choice of input variables and the precise definition of desired outputs are crucial for attaining optimal model performance. An extensive set of input variables is systematically gathered from published literature [22]. It is important to reiterate, as highlighted in multiple references, including [23], that the pile's dimensions, particularly its length and diameter, play a paramount role in determining the Q_u. Therefore, to consider the impact of rock and soil layers, 2 ratios associated with pile geometry were chosen: the ratio of length within the soil layer (Ls) to socket length (Lr), and the ratio of total length (Lt) to diameter (D).

In summary, the model inputs for estimating the Q_u of rock-socketed piles consisted of $Ls/Lr, Lt/D, UCS,$ and $SPT\ N$ −value. In addition, Hr is the height of the layer. These inputs were chosen to simplify the predictive model using smaller parameters. Table I indicates the statistical properties of these inputs and Q_u. Fig. 1 presents a column plot for determining the input frequency in correlation with Q_u.

TABLE I. The Statistical Properties of the Input Variable of Q_u

Variables		Indicators			
	Category	***Min***	***Max***	***Avg***	***St. Div***
Lp/D	Input	4.331	96.30	31.39	22.57
Ls/Lr	Input	0.29	31.71	4.86	5.66
N_SPT	Input	0.00	166.42	44.67	59.57
UCS	Input	0.00	68.49	24.23	23.55
Hr	Input	0.00	8.36	0.79	1.50
Qu	Output	1449.00	42700.73	17421.79	10230.86

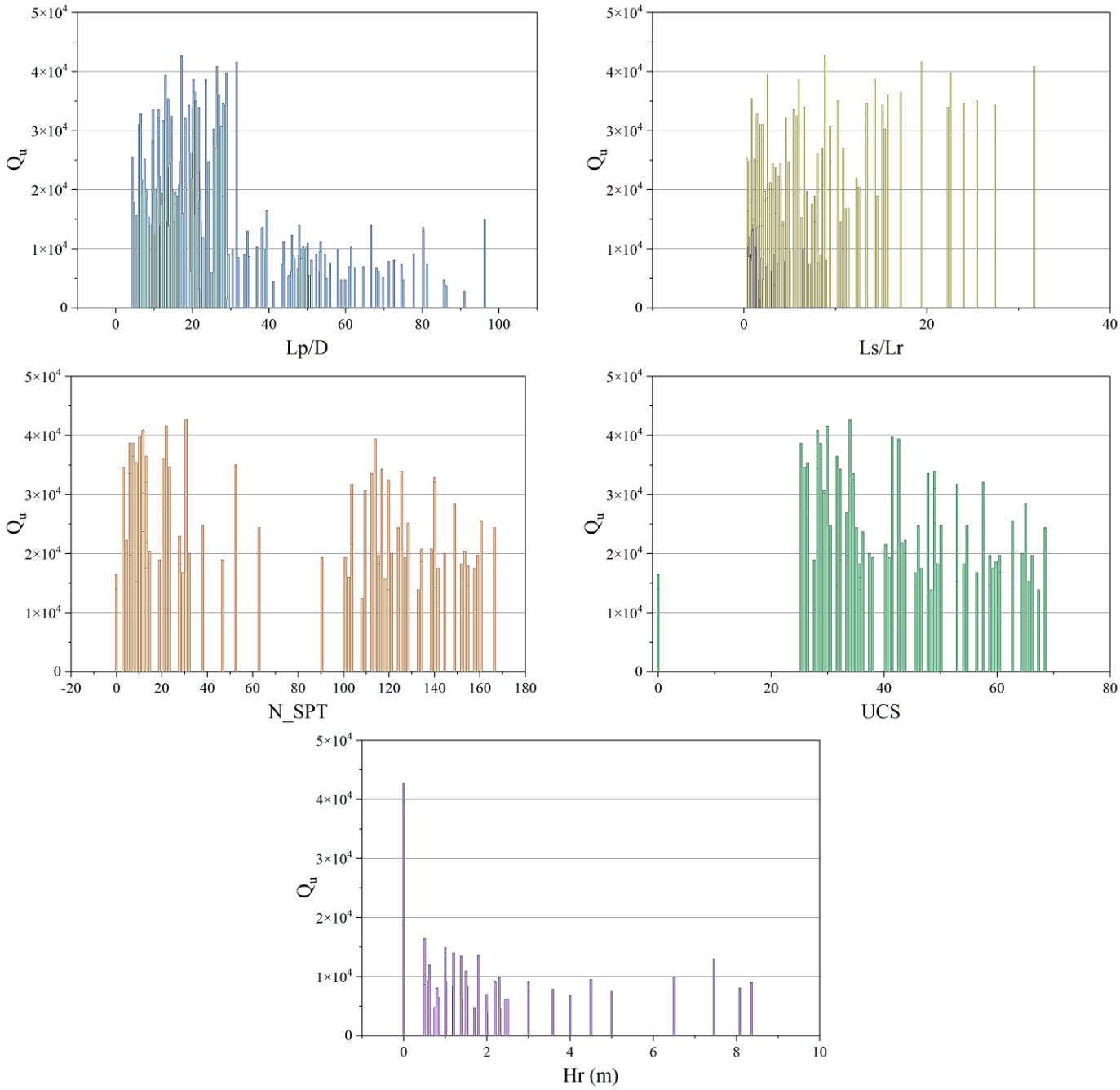

Fig. 1. The column plot between input and output.

B. DT

Derived from ML theory, a DT functions as a potent instrument for proficiently tackling regression and classification challenges. In contrast to other classification techniques that rely on a combined set of features for one-step classification, the DT employs a multi-stage or hierarchical decision approach, displaying a structure resembling a tree [24]. In contrast to other classification methods that depend on a unified set of features for immediate classification, the DT employs a multi-stage or hierarchical decision approach, showcasing a structure that resembles a tree. This tree includes a root node housing all the data, a sequence of splits (*internal nodes*) , and an assortment of leaves (*terminal nodes*) [25]. Within the DT structure, each node performs a binary decision, separating either a singular class or a subset of classes from the remaining ones. Typically, the process entails traversing the tree from the top to the bottom, following a top-down methodology [26].

1) Decision tree regression (DTR): As shown in Fig. 2, a distinct regression tree is built for every class to enable soft classification. Within the context of regression trees, the target vector is the defined class proportions of a pixel, also known as soft reference data, whilst the pixel intensity values from

various bands function as estimator feature vectors or variables. The technique generates predicted class proportions as an output by using the intensity values as input for each individual regression tree [27]. The steps involved in creating regression trees using the training dataset are as follows:

a) Employ the pixel intensity values from different bands as the variables that predict.

b) Employ the known class fraction of class i within the target variable, a pixel.

c) Create the regression tree specific to class i.

d) Iterate through the process for class i, varying from 1 to M.

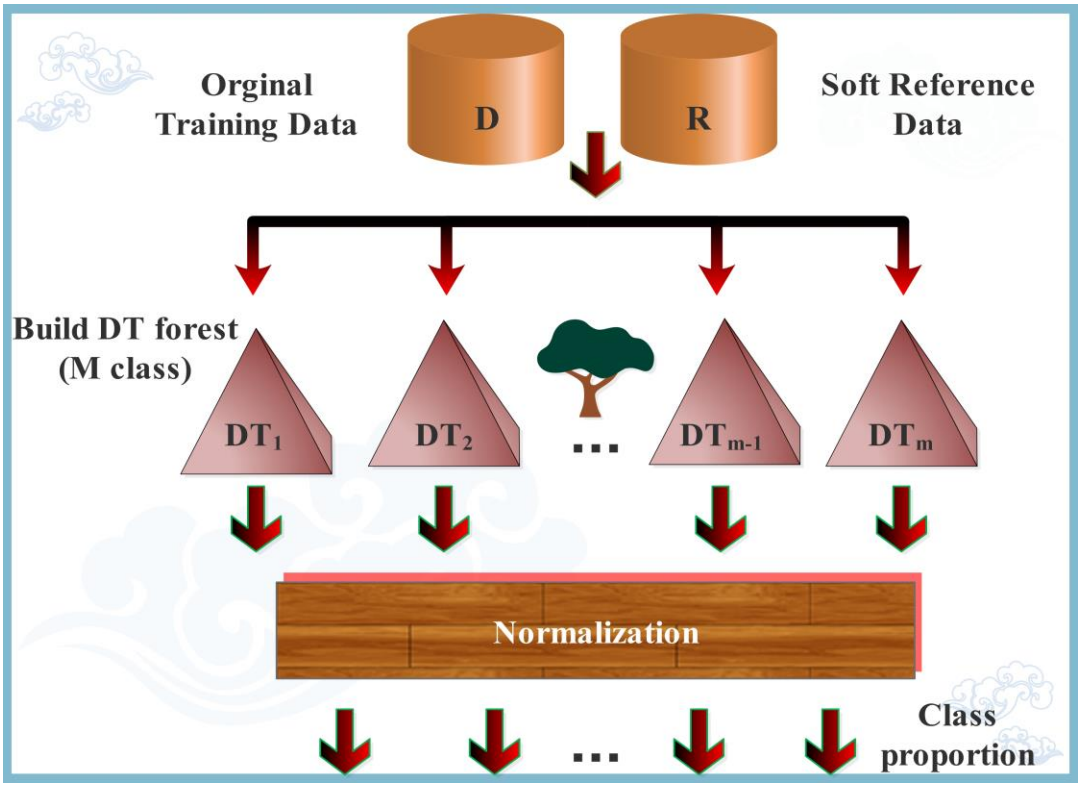

Fig. 2. The DT regression technique facilitates the soft classification of remote sensing data.

The regression tree algorithm for soft categorization is as follows:

1) Input the pixel intensity values from various bands.

2) Execute the regression tree for class i.

3) Retrieve the output of regression tree i, which represents the fraction of class i in a pixel.

4) Repeat the process for class i, ranging from 1 to M.

It is common practice to rescale the soft classification outputs to a range of 0 to 1 for each pixel, indicating the class fractions within the ground pixel area. Thus, the estimated class proportions from each tree, denoted as $DT(i)\ for\ i = 1,\dots,M$, undergo normalization through the following process:

$$P(i) = \frac{DT(i)}{\sum DT(i)}, i = 1, \dots, M \quad (1)$$

C. Zebra Optimization Algorithm (ZOA)

Zebras are included in the cohort population of ZOA, a population-based optimization method. It updates its members by utilizing 2 innate behaviors seen in wild zebras. These include hunting and gathering food as well as protecting oneself from predators. Therefore, the ZOA population members receive updates in 2 distinct stages for each iteration [28].

1) Foraging behavior: Zebras predominantly graze on grasses and sedges; however, they might turn to buds, bark, fruits, roots, and leaves when their preferred food is scarce. During the initial stage, updates to the population members are executed by simulating zebra behavior while searching for food. The amount of time zebras dedicate to eating can vary between 60-80 percent, contingent on the quality and accessibility of vegetation. Among zebras, the plains zebra stands out as a primary grazer. It consumes the upper canopy of grass, which is often less nutritious, creating an environment conducive for other species that rely on Shorter and more nutrient-rich grasses. In ZOA [29], the lead zebra is regarded as the top-performing member of the population and directs other members toward its location in the search area. Consequently, the adjustment of zebra positions during the foraging stage can be expressed mathematically utilizing Eq. (2) and (3).

$$x_{i,j}^{new,p_1} = x_{i,j} + e \times (BM_j - I \times x_{i,j}) \quad (2)$$

$$x_i = \begin{cases} x_i^{new,p_1}, F_i^{new,p_1} < f_i \\ x_i \qquad otherwise \end{cases} \quad (3)$$

In this context, x_i^{new,p_1} represents the updated state of the ith zebra, with $x_{i,j}^{new,p_1}$ denoting its value in the jth dimension and F_i^{new,p_1} indicating its updated objective function value. The lead zebra, referred to as BM, stands as the top-performing member, and BM_j signifies its value in the jth dimension [30]. The value of i is determined using a random number e, which can be any value between 0 and 1. The round function $(1 + rand)$ is then used to round the value of i to the closest integer. The parameter i has 2 possible values: 1 and 2. Setting i to 2 results in more significant changes in population mobility.

2) Defense strategies against predators: Updates to the positions of ZOA residents in the search area are made in the second stage by using simulations of a zebra's defensive maneuvers against predator attacks. Not only do lions pose a threat to zebras, but wild dogs, leopards, brown hyenas, and cheetahs also pose a hazard, each of which calls for a different approach to defense. Zebras defend themselves against lion attacks by using zigzag patterns and occasional sideways spins as evasive maneuvers. Zebras usually react more aggressively to smaller predators such as hyenas and dogs. They regroup and cause chaos to make their enemies more difficult to deal with. In the context of ZOA, the assumption is that lions or other predators may initiate an attack, prompting zebras to decide between an escape strategy when facing lions or an offensive approach against other predators [31]. The escape strategy is represented by mode S1, while the defensive strategy, where the herd forms a protective structure, is represented by mode S2. A zebra's new position is valid if it results in an improved objective function value.

$$x_{i,j}^{new,p_2} = \begin{cases} S1: x_{i,j} + E \times (2e-1) \times \left(1 - \frac{t}{T}\right) \times x_{i,j}, P_s \leq 0.5 \\ S2: x_{i,j} + e \times \left(BM_j - I \times x_{i,j}\right), \qquad otherwise \end{cases} \quad (4)$$

$$x_i = \begin{cases} x_i^{new,p_2}, F_i^{new,p_2} < f_i \\ x_i \qquad otherwise \end{cases} \quad (5)$$

In this context, the constant E is fixed at 0.01, and P_s represents the likelihood of selecting one of two methods at random from the range [0,1]. BM refers to the condition of the zebra under attack, where BM_j signifies its value in the jth dimension.

D. Coronavirus Herd Immunity Optimizer (CHIO)

The algorithm for optimization introduced in this study integrates the concept of herd immunity, drawing parallels between the principles of $COVID-19$ and the optimization process [32]. The steps that make up the $CHIO$ are listed below, with a detailed explanation of each. The algorithm explores each of the 6 primary phases in the parts that follow [33, 34].

Phase 1: To fit the optimization difficulty's context, the objective function is formulated as follows during the $CHIO$ and optimization problem's initialization phase:

$$minO(x) \quad x \in [lb, ub] \quad (6)$$

An individual's or case $x's$ immunity rate is reflected by the objective function $O(x)$, which is denoted by the gene values $x_1, x_2, \ldots, x_n$, where each x_i corresponds to a gene or choice variable. Each person's total gene count is denoted by the index n. It is crucial to emphasize that each gene x_i falls within the value range of $[lb_i, ub_i]$, with ub_i and lb_i denoting the $upper$ and $lower$ boundaries, respectively, of gene x_i.

Through this phase, CHIO initializes its two primary control parameters [34]: BR_r, It governs the propagation of the virus pandemic among people and acts as the fundamental reproduction rate governing the $CHIO$ operators. Max_{age}, This denotes the oldest age at which infected cases can be documented and describes how those instances will end. Cases reaching Max_{age} either recover or pass away.

Two control parameters and $four$ algorithmic parameters make up $CHIO$. C_0: This is the initial number of infected instances, which in this particular case is one. Max_{it}: the highest quantity of repetitions. HIS: The number of people. n: The problem's dimensionality.

Phase 2: The examples that are generated are then saved in HIP in the form of a 2-dimensional matrix with dimensions of $n\ x\ HIS$. Here, n stands for each person's size, which is indicated as follows:

$$HIP = \begin{bmatrix} x_1^1 & x_2^1 & \cdots & x_n^1 \\ x_1^2 & x_1^2 & \cdots & x_n^2 \\ \vdots & \vdots & \cdots & \vdots \\ x_1^{HIS} & x_2^{HIS} & \cdots & x_n^{HIS} \end{bmatrix} \quad (7)$$

Each row in HIP denoted as x_j, fits a case that is produced by the following formula: $x_i^j = lb_i + (ub_i - lb_i) \times U(0,1)$, where i series from 1 to n, and where ub_i and lb_i represent the $upper$ and $lower$ limitations of the gene x_i. Eq. (6) is utilized to calculate the immunity rate, or objective function, for every instance. Every instance in HIP also has a status vector (S) constructed for it, with a length of HIS. In this vector, a vulnerable case is represented by 0, and an infected case is represented by 1 value.

Phase 3: The progression of coronavirus herd protection constitutes the central iterative process of $CHIO$. This process encompasses $three$ rules governing the change of genes x_i^j within case x_j. These genes can either remain unchanged or undergo alterations due to the implementation of social estrangement procedures. The specific rules are strongminded according to the percentage of BR_r and are detailed as follows:

$$x_i^j(t+1) \leftarrow \begin{cases} x_i^j(t) & r \geq BR_r \\ C\left(x_i^j(t)\right) & r < \frac{1}{3} \times BR_r. \quad infected \\ N\left(x_i^j(t)\right) & r < \frac{2}{3} \times BR_r. \quad suspectical \\ R\left(x_i^j(t)\right) & r < BR_r. \quad immuned \end{cases} \quad (8)$$

Phase 4: The immunity rate, denoted as $O(x^j(t+1))$, is computed for each newly generated case, $x^j(t+1)$. If it outperforms the current case, $x^j(t)$, as indicated by $(x^j(t+1)) > O(x^j(t))$, then $x^j(t)$ is substituted with $x^j(t+1)$. Furthermore, if $E_j = 1$, the age vector A^j is incremented by one.

The status vector, E_j, for each case, x^j, is adjusted based on the herd immunity threshold, calculated as follows:

$$E_j \leftarrow \begin{cases} 1 & O\left(x^j(t+1)\right) < \frac{O(x^j)(t+1)}{\Delta O(x)}, E_j = 0, is\_corona(x^j(t+1)) \\ 2 & O\left(x^j(t+1)\right) < \frac{O(x^j)(t+1)}{\Delta O(x)}, E_j = 1 \end{cases} \quad (9)$$

The equation is formulated based on the following variables:

- $is_{corona}(x^j(t+1))$: A dual value set to 1 if the newly created case, $x^j(t+1)$ inherits an amount from each affected instance.
- ΔO(x): This denotes the mean immunity rate of the population, which is calculated as the sum of all immunity rates divided by the population size.

It is crucial to stress that determined social distancing measures may have an impact on the population's immunity rate among persons [35], considering that the freshly formed individual's immunity rate is higher than the population's average immunity rate.

E. Performance Evaluator

This section delineates a set of metrics designed to assess hybrid models. These metrics gauge error and correlation, providing respected insights into the models' performance. Table II displays the equations for the metrics employed in this paper [36].

Respectively, the variables can be expressed as:

- The symbol n represents the sample size.
- Predicted values are indicated as b_i.
- $\bar{m}$ and $\bar{b}$ stand for the mean of the evaluated and anticipated values, respectively.
- The measured value is denoted as m_i.
- The mean of the predictor variable in the dataset is symbolized as $\bar{x}$.

TABLE II. THE FORMULATIONS OF THE PERFORMANCE METRICS

Coefficient Correlation (R^2):	$\boldsymbol{R^2} = \left(\frac{\sum_{i=1}^{n}(\boldsymbol{b_i} - \bar{\boldsymbol{b}})(\boldsymbol{m_i} - \bar{\boldsymbol{m}})}{\sqrt{\left[\sum_{i=1}^{n}(\boldsymbol{b_i} - \bar{\boldsymbol{b}})^2\right]\left[\sum_{i=1}^{n}(\boldsymbol{m_i} - \bar{\boldsymbol{m}})^2\right]}} \right)^2$	(10)
Root Mean Square Error (RMSE):	$RMSE = \sqrt{\frac{1}{n}\sum_{i=1}^{n}(m_i - b_i)^2}$	(11)
Mean Absolute Error (MAE):	$MAE = \frac{1}{n}\sum_{i=1}^{n}\lvert b_i - m_i \rvert$	(12)
Mean Absolute Percentage Error (MAPE):	$MAPE = \frac{100}{n}\sum_{i}^{n}\frac{\lvert b_i \rvert}{\lvert m_i \rvert}$	(13)
weight absolute percentage error (WAPE):	$WAPE = \max\left[\frac{\lvert b_i - m_i \rvert}{b_i}\right]$	(14)

III. RESULT

In this section, a comparative assessment of the results was carried out to obtain the proposed model using single and hybrid frameworks. The hybrid variants developed to achieve optimal outcomes include DT+ZOA (DTZO) and DT+CHIO (DTCH). To train these proposed models, 70% of the input data was dedicated to the training process, while the remaining 30% was further divided, with 15% allocated for validation and 15% for testing purposes. Various metrics, including R2, RMSE, MAE, MAPE, and WAPE, were employed to conduct a thorough assessment of the acquired results and ensure unbiased findings. In the case of the R2 metric, values close to 1 suggest excellent results. Conversely, values approaching 0 indicate accurate outcomes when considering the error indicators.

Table III presents the results of predicting the Q_u of rocks for each framework. The performance of the traditional DT models within a single framework does not show favorable outcomes according to the mentioned metrics. While the R2 value for DT is 0.9817 during the training phase, it notably decreases in both the validation and testing phases. On the other hand, DTZA exhibits steady performance, especially in the training phase, with an R2 value of 0.9962 and an RMSE value of 629.7812. Among the models, the DTCH model showed moderate results, achieving higher accuracy compared to DT but slightly lower accuracy than the DTZA model. Overall, it can be concluded that the accuracy of DT models in predicting the Q_u of rocks is successfully enhanced by the incorporation of ZOA and CHIO optimizers, which contributes to an overall improvement in the reliability of the results.

Fig. 3 displays a scatter plot depicting the models' performance, evaluated through their R^2 and RMSE values. The X-axis correlates with the measured values, while the Y-axis correlates with the predicted values generated by the models. Triangular shapes in various colors are incorporated into the scatter plot to distinguish between the training, testing, and validation phases. These shapes are dispersed around a

diagonal line, representing an ideal scenario with an R^2 value of 1. The limited accuracy of the DT model becomes apparent due to the significant spread of data points.

Conversely, the DTZA and DTCH models demonstrate enhanced performance compared to the standalone DT approach. Data points for DTZA are tightly clustered near the central line, indicating a more favorable outcome. However, some broader dispersions are observable in the case of DTCH.

TABLE III. THE RESULT OF DEVELOPED MODELS FOR DT

Model	Phase	Index values				
		RMSE	***R^2***	***MAE***	***MAPE***	***WAPE***
DT	Train	1440.54	0.9817	1235.19	11.3086	0.0713
	Validation	1829.53	0.9683	1471.95	7.6086	0.0726
	Test	1695.50	0.9746	1121.61	7.4247	0.0745
	All	1545.41	0.9774	1253.81	10.1622	0.0720
DTZA	Train	629.78	0.9962	446.47	2.6926	0.0258
	Validation	1221.55	0.9873	926.96	4.6943	0.0457
	Test	1229.66	0.9893	814.87	5.2731	0.0541
	All	854.89	0.9934	574.80	3.3853	0.0330
DTCH	Train	1001.70	0.9903	742.39	4.6906	0.0429
	Validation	1503.80	0.9806	1145.34	5.7609	0.0565
	Test	1250.77	0.9834	850.54	5.7691	0.0604
	All	1178.30	0.9872	841.02	5.0565	0.0483

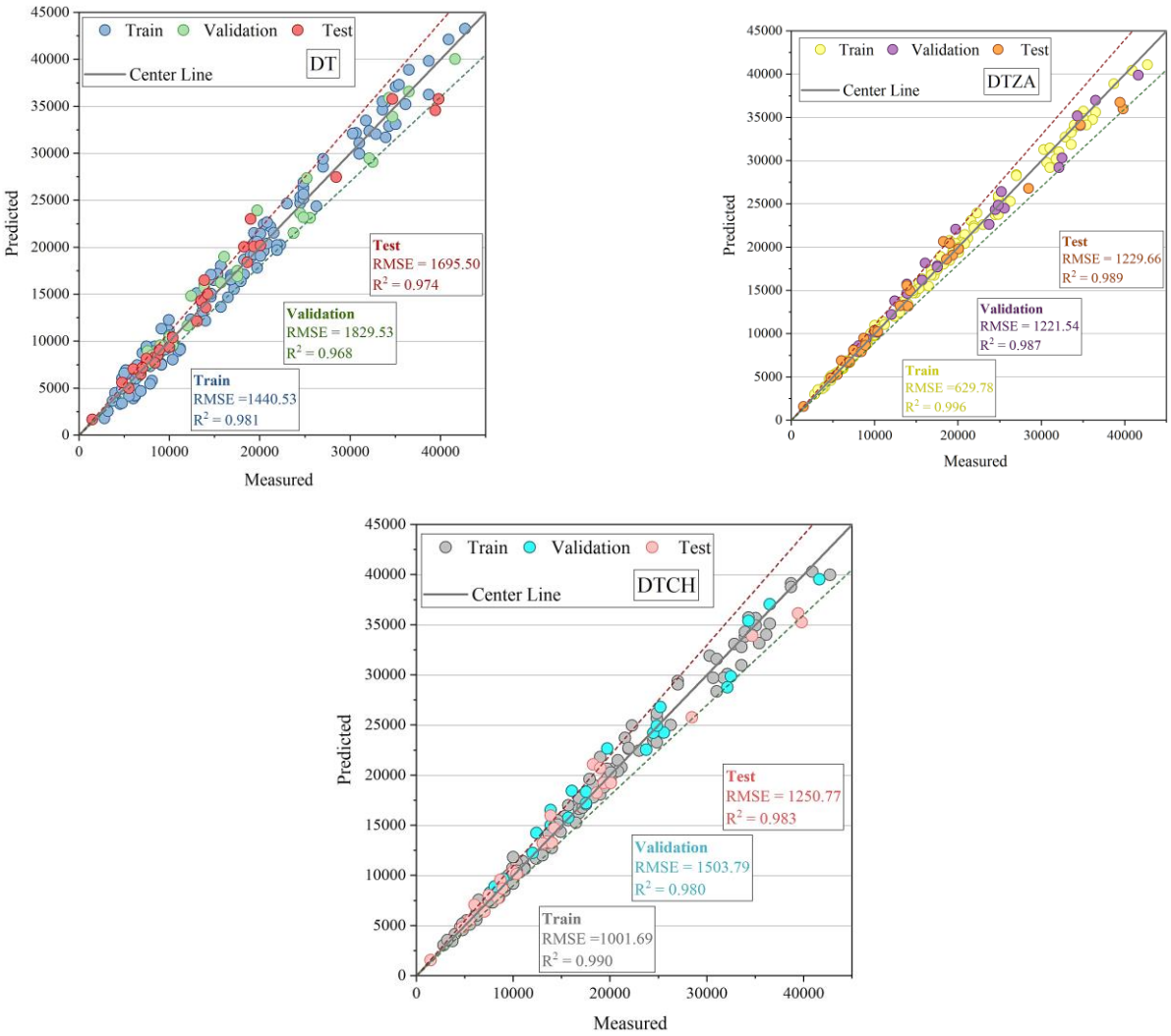

Fig. 3. The correlation between the predicted and measured values.

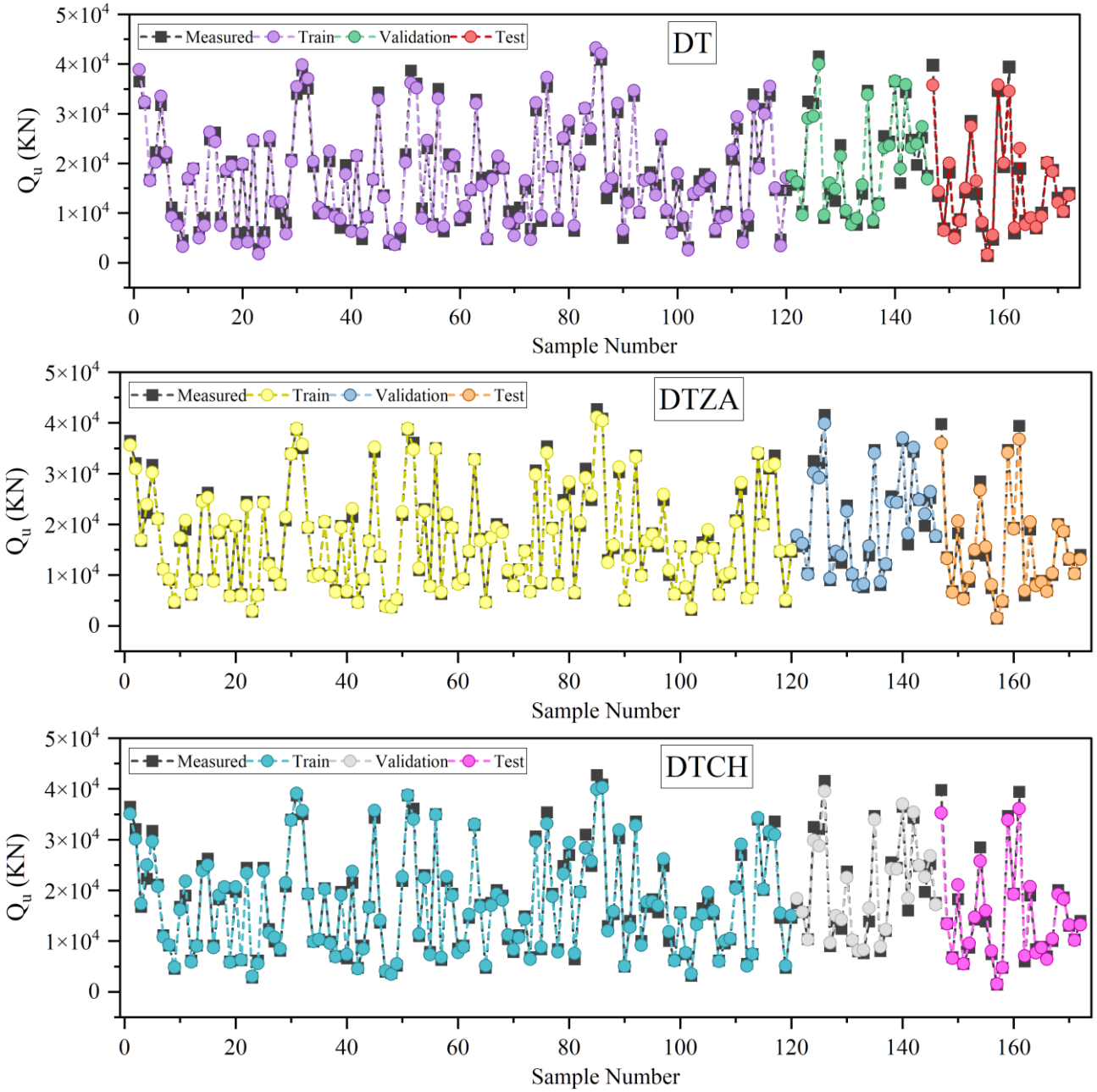

Fig. 4. The comparison of measured and predicted values.

Fig. 4 presents the relationship between predicted and measured values of the DT base models. In this figure, the measured values are represented by the black box. When the predicted values closely align with these measured values, it signifies the model's accuracy. As shown in Fig. 4, the DT model exhibits a significant deviation of its data from the measured values, particularly during the testing phase. Conversely, the DTZA model showcases a precise outcome, with an almost perfect match between its predicted and measured values, particularly within the sample numbers from 40 to 80. In contrast, the DTCH model demonstrates a noticeable lack of accuracy within the sample numbers ranging from 80 to 120, rendering it less precise than the DTZA model.

It is crucial to conduct an error assessment to achieve a deeper understanding of the uniqueness and precision of the models. Fig. 5 emphasizes that the DT model displayed a significant error rate, especially during the testing phase, peaking at a maximum error of 35% within the sample range of 0 to 50. On the other hand, most data points in the DTZA model exhibited errors that were nearly 0%, in contrast to the DTCH model, where the maximum error reached 20%.

Fig. 6 presents a box plot that simplifies the comparison of errors among the models within a single visual representation. The precision of the DTZA model becomes evident as the data points are closely grouped, primarily concentrated within the error range of -5% to 5%. This pattern contrasts with the

spread seen in the other models, underscoring the dependability of the DTZA model's predictions. The concentration of data points within a relatively narrow error range signifies its consistent and accurate performance. In contrast, the dispersion observed in the error distribution of the other models indicates a broader variability in their predictions.

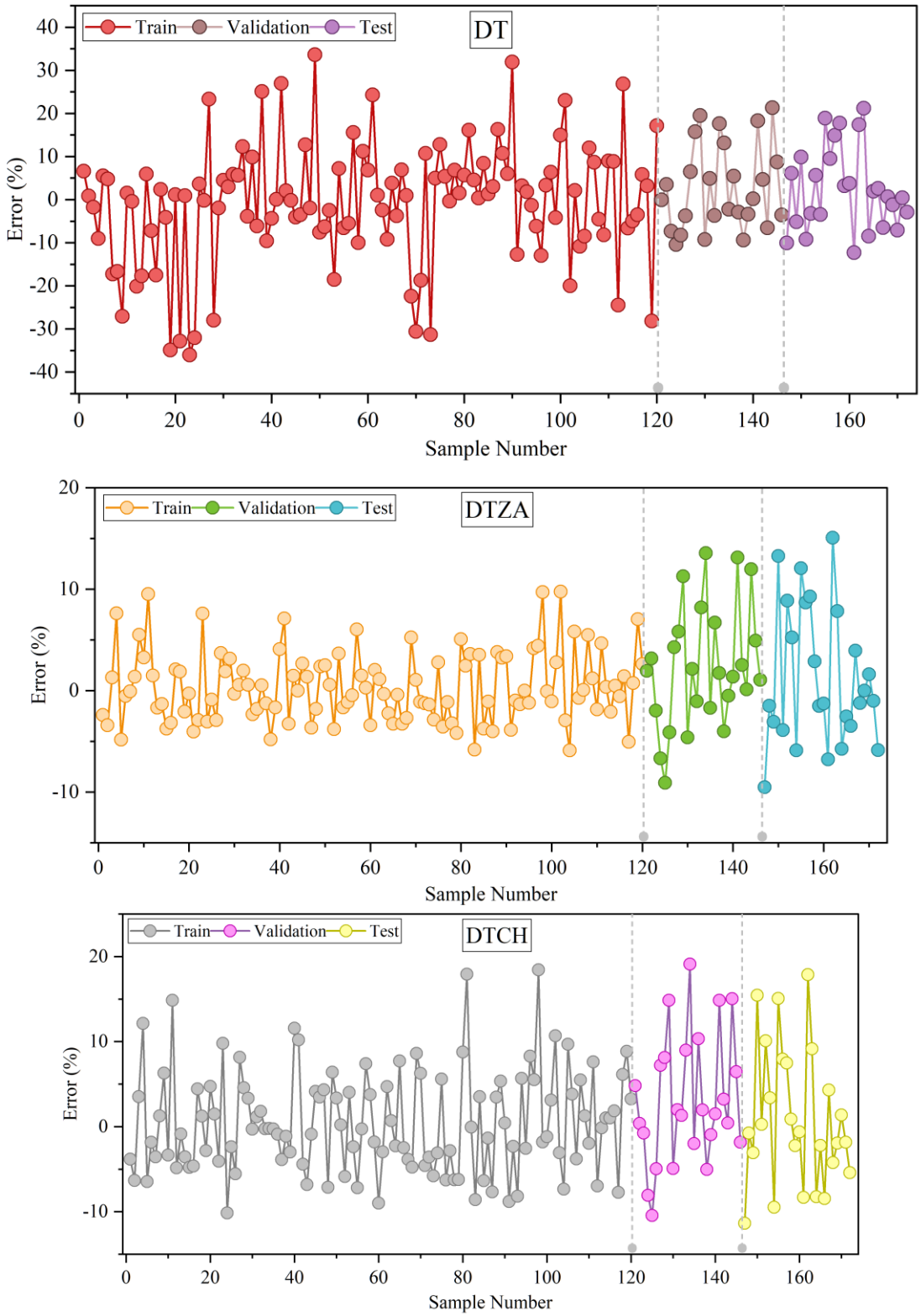

Fig. 5. The error percentage for the hybrid models is based on a line-symbol plot.

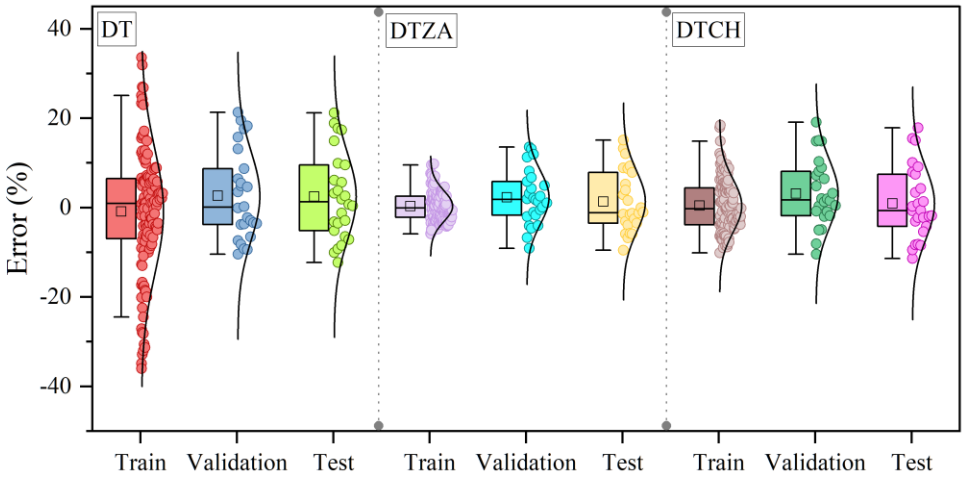

Fig. 6. The box plot of errors among the developed models.

IV. Discussion

A. Comparison between the Results of Previous Articles and the Present Study

Table IV presents the results of previous research efforts on Qu prediction, providing a comprehensive benchmark for comparison with the current study. Among the five models discussed in this table from earlier research, the GA-DLNN model, described in Pham et al.'s research [37], demonstrated the most impressive performance, achieving an R^2 of 0.882 and an RMSE of 109.965. As detailed in the previous Section, the current investigation emphasizes the superior performance of the DTZA model during the training phase, producing commendable metric scores with an R^2 value of 0.9962 and an RMSE of 629.78. This exceptional performance in critical metrics decisively positions the DTZA model in this study as outperforming its counterparts, confirming its effectiveness in Qu prediction.

TABLE IV. Comparing the Results of the Present Study with Previous Studies

Articles	Models	Models' performance	
		RMSE	R^2
Armaghani et al. [38]	ANN	0.135	0.808
Pham et al. [37]	GA-DLNN	109.965	0.882
Momeni et al. [39]	ANN	0.529	0.71
Momeni et al. [39]	ANFIS	0.048	0.875
Kulkarni et al. [40]	GA-ANN	0.0093	0.86
Present Study	DTZA (DT+ZAO)	629.78	0.9962

B. Results of an Ablation Study

In this study, an ablation study was conducted as an alternative assessment approach. Two input values, as detailed in previous sections, were deliberately removed from the dataset. Subsequently, the prediction process was reiterated utilizing the best hybrid model. The outcomes of this ablation study were then compared with those of the main prediction process, with the findings summarized in Table V. Analysis of the table reveals that the results of the Main Study outperformed those of the Ablation Study. Specifically, the Root Mean Square Error (RMSE) of the Main Study was 17.22% lower than that of the Ablation Study, indicating a superior predictive performance in the former.

TABLE V. Comparing the Results of the Main Study with Ablation Study

phase	Main Study		Ablation Study	
	R^2	RMSE	R^2	RMSE
Train	0.9962	629.78	0.9942	774.33
Validation	0.9873	1221.55	0.9818	1464.26
Test	0.9893	1229.66	0.9845	1470.84
All	0.9934	854.89	0.9904	1032.73

C. Limitations of the Study

The study's limitations are acknowledged, including the potential restriction of results' generalizability by the specific dataset and experimental setup utilized. Variations in geological conditions, pile types, and other site-specific factors could affect the performance of the proposed hybrid models in different contexts. Additionally, the focus on predictive accuracy in the analysis may neglect considerations of computational efficiency or scalability, which could be crucial in real-world applications. Furthermore, biases or uncertainties may be introduced by the assumptions and parameters chosen for the optimization algorithms. Lastly, while efforts were made to provide insightful analysis of the experimental results, there may be aspects that require further investigation or validation in future studies. These limitations underscore the need for a cautious interpretation of the findings and highlight avenues for future research to address these constraints and refine the proposed methodologies.

V. Conclusion

The estimation of the ultimate bearing capacity (Q_u) using ML methods, specifically the DT model, coupled with advanced optimization algorithms, including the Zebra Optimization Algorithm (ZOA) and the Coronavirus Herd Immunity Optimizer (CHIO), has demonstrated significant promise and yielded valuable insights into the field of civil engineering. The incorporation of ML techniques, particularly the DT model, has proven to be a powerful tool for accurately estimating the ultimate bearing capacity of soils and rocks. The

utilization of this model allows for the efficient handling of complex datasets and the extraction of meaningful patterns and relationships within the data. However, as revealed in the analysis, the standalone DT model exhibited limitations in accuracy, especially during the testing phase, highlighting the need for further refinement. The fusion of the DT model with optimization algorithms, such as ZOA and CHIO, has been a pivotal advancement in enhancing predictive accuracy. The ZOA and CHIO optimizers have contributed to refining the model's performance during the training, validation, and testing phases. The analysis of the prediction results, as depicted in correlation and error assessments, showcased the distinctiveness of these models. The DTZA model demonstrated remarkable accuracy, with a close alignment between predicted and measured values. Its ability to maintain errors close to 0% over a wide range of samples is a testament to its consistent and precise performance. On the other hand, the DTCH model, while showing improved accuracy compared to the standalone DT model, exhibited some variability in its predictions, particularly in a specific sample range. The integration of ML methods, DT models, and advanced optimization algorithms like ZOA and CHIO has proven to be a valuable approach for predicting the ultimate bearing capacity in civil engineering applications. These hybrid models have shown substantial improvements in accuracy and reliability, which are crucial for making informed decisions in geotechnical engineering projects. Further research and fine-tuning of these models can advance the understanding and predictive capabilities in civil engineering, particularly in earthquake analysis and related areas.

ACKNOWLEDGMENTS

2023 Jilin Provincial Department of Education Science Research Project, Project Name: "Studying on the Shrinkage Behavior of Semi-flexible Grading Gravel Base Material in Cold Regions" (Project Number: JJKH20231038KJ)

REFERENCES

[1] Cai G, Liu S, Tong L, Du G. Assessment of direct CPT and CPTU methods for predicting the ultimate bearing capacity of single piles. Eng Geol 2009;104:211–22.

[2] Yong W, Zhou J, Jahed Armaghani D, Tahir MM, Tarinejad R, Pham BT, et al. A new hybrid simulated annealing-based genetic programming technique to predict the ultimate bearing capacity of piles. Eng Comput 2021;37:2111–27.

[3] Harandizadeh H, Toufigh V. Application of developed new artificial intelligence approaches in civil engineering for ultimate pile bearing capacity prediction in soil based on experimental datasets. Iranian Journal of Science and Technology, Transactions of Civil Engineering 2020;44:545–59.

[4] Chen W, Sarir P, Bui X-N, Nguyen H, Tahir MM, Jahed Armaghani D. Neuro-genetic, neuro-imperialism and genetic programing models in predicting ultimate bearing capacity of pile. Eng Comput 2020;36:1101–15.

[5] Rock ACD-18 on S. Standard Test Methods for Laboratory Compaction Characteristics of Soil Using Modified Effort (56,000 Ft-Lbf/Ft3 (2,700 KN-M/M3)) 1. ASTM international; 2009.

[6] Pham TA, Ly H-B, Tran VQ, Giap L Van, Vu H-LT, Duong H-AT. Prediction of pile axial bearing capacity using artificial neural network and random forest. Applied Sciences 2020;10:1871.

[7] Masoumi F, Najjar-Ghabel S, Safarzadeh A, Sadaghat B. Automatic calibration of the groundwater simulation model with high parameter dimensionality using sequential uncertainty fitting approach. Water Supply 2020;20:3487–501. https://doi.org/10.2166/ws.2020.241.

[8] Akbarzadeh MR, Ghafourian H, Anvari A, Pourhanasa R, Nehdi ML. Estimating Compressive Strength of Concrete Using Neural Electromagnetic Field Optimization. Materials 2023;16:4200.

[9] Yagiz S, Sezer EA, Gokceoglu C. Artificial neural networks and nonlinear regression techniques to assess the influence of slake durability cycles on the prediction of uniaxial compressive strength and modulus of elasticity for carbonate rocks. Int J Numer Anal Methods Geomech 2012;36:1636–50.

[10] Jahed Armaghani D, Tonnizam Mohamad E, Hajihassani M, Yagiz S, Motaghedi H. Application of several non-linear prediction tools for estimating uniaxial compressive strength of granitic rocks and comparison of their performances. Eng Comput 2016;32:189–206.

[11] Singh R, Kainthola A, Singh TN. Estimation of elastic constant of rocks using an ANFIS approach. Appl Soft Comput 2012;12:40–5.

[12] Shirani Faradonbeh R, Monjezi M, Jahed Armaghani D. Genetic programing and non-linear multiple regression techniques to predict backbreak in blasting operation. Eng Comput 2016;32:123–33.

[13] Monjezi M, Hasanipanah M, Khandelwal M. Evaluation and prediction of blast-induced ground vibration at Shur River Dam, Iran, by artificial neural network. Neural Comput Appl 2013;22:1637–43.

[14] Marto A, Hajihassani M, Jahed Armaghani D, Tonnizam Mohamad E, Makhtar AM. A novel approach for blast-induced flyrock prediction based on imperialist competitive algorithm and artificial neural network. The Scientific World Journal 2014;2014.

[15] Azimi M, Molaei Yeznabad A. Swarm-based Parallel Control of Adjacent Irregular Buildings Considering Soil–structure Interaction. Journal of Sensor and Actuator Networks 2020;9. https://doi.org/10.3390/jsan9020018.

[16] Pal M, Deswal S. Modeling pile capacity using support vector machines and generalized regression neural network. Journal of Geotechnical and Geoenvironmental Engineering 2008;134:1021–4.

[17] Shahin MA, Jaksa MB, Maier HR. Recent advances and future challenges for artificial neural systems in geotechnical engineering applications. Advances in Artificial Neural Systems 2009;2009.

[18] Jianbin Z, Jiewen T, Yongqiang S. An ANN model for predicting level ultimate bearing capacity of PHC pipe pile. Earth and Space 2010: Engineering, Science, Construction, and Operations in Challenging Environments, 2010, p. 3168–76.

[19] Lei Y, Zhou S, Luo X, Niu S, Jiang N. A comparative study of six hybrid prediction models for uniaxial compressive strength of rock based on swarm intelligence optimization algorithms. Front Earth Sci (Lausanne) 2022;10.

[20] Agushaka JO, Ezugwu AE. Advanced arithmetic optimization algorithm for solving mechanical engineering design problems. PLoS One 2021;16:e0255703.

[21] Dhiman G, Singh KK, Soni M, Nagar A, Dehghani M, Slowik A, et al. MOSOA: A new multi-objective seagull optimization algorithm. Expert Syst Appl 2021;167:114150.

[22] Jahed Armaghani D, Shoib RSNSBR, Faizi K, Rashid ASA. Developing a hybrid PSO–ANN model for estimating the ultimate bearing capacity of rock-socketed piles. Neural Comput Appl 2017;28:391–405.

[23] Momeni E, Nazir R, Armaghani DJ, Maizir H. Prediction of pile bearing capacity using a hybrid genetic algorithm-based ANN. Measurement 2014;57:122–31.

[24] Erdal HI. Two-level and hybrid ensembles of decision trees for high performance concrete compressive strength prediction. Eng Appl Artif Intell 2013;26:1689–97.

[25] Patel N, Upadhyay S. Study of various decision tree pruning methods with their empirical comparison in WEKA. Int J Comput Appl 2012;60.

[26] Karbassi A, Mohebi B, Rezaee S, Lestuzzi P. Damage prediction for regular reinforced concrete buildings using the decision tree algorithm. Comput Struct 2014;130:46–56.

[27] Ke G, Meng Q, Finley T, Wang T, Chen W, Ma W, et al. Lightgbm: A highly efficient gradient boosting decision tree. Adv Neural Inf Process Syst 2017;30.

[28] Trojovská E, Dehghani M, Trojovský P. Zebra optimization algorithm: A new bio-inspired optimization algorithm for solving optimization algorithm. IEEE Access 2022;10:49445–73.

[29] Mohapatra S, Mohapatra P. American zebra optimization algorithm for global optimization problems. Sci Rep 2023;13:5211.

[30] Rana A, Khurana V, Shrivastava A, Gangodkar D, Arora D, Dixit AK. A ZEBRA Optimization Algorithm Search for Improving Localization in Wireless Sensor Network. 2022 2nd International Conference on Technological Advancements in Computational Sciences (ICTACS), IEEE; 2022, p. 817–24.

[31] Zare P, Davoudkhani IF, Zare R, Ghadimi H, Mohajeri R, Babaei A. Maiden Application of Zebra Optimization Algorithm for Design PIDN-TIDF Controller for Frequency Control in Offshore Fixed Platforms Microgrid in the Presence of Tidal Energy. 2023 8th International Conference on Technology and Energy Management (ICTEM), IEEE; 2023, p. 1–7.

[32] Al-Betar MA, Alyasseri ZAA, Awadallah MA, Abu Doush I. Coronavirus herd immunity optimizer (CHIO). Neural Comput Appl 2021;33:5011–42.

[33] Alweshah M, Alkhalaileh S, Al-Betar MA, Bakar AA. Coronavirus herd immunity optimizer with greedy crossover for feature selection in medical diagnosis. Knowl Based Syst 2022;235:107629.

[34] Dalbah LM, Al-Betar MA, Awadallah MA, Zitar RA. A modified coronavirus herd immunity optimizer for capacitated vehicle routing problem. Journal of King Saud University-Computer and Information Sciences 2022;34:4782–95.

[35] Amini S, Ghasemi S, Golpira H, Anvari-Moghaddam A. Coronavirus herd immunity optimizer (CHIO) for Transmission Expansion Planning. 2021 IEEE International Conference on Environment and Electrical Engineering and 2021 IEEE Industrial and Commercial Power Systems Europe (EEEIC/I&CPS Europe), IEEE; 2021, p. 1–6.

[36] Botchkarev A. Performance metrics (error measures) in machine learning regression, forecasting and prognostics: Properties and typology. ArXiv Preprint ArXiv:180903006 2018.

[37] Pham TA, Tran VQ, Vu H-LT, Ly H-B. Design deep neural network architecture using a genetic algorithm for estimation of pile bearing capacity. PLoS One 2020;15:e0243030.

[38] Jahed Armaghani D, Shoib RSNSBR, Faizi K, Rashid ASA. Developing a hybrid PSO–ANN model for estimating the ultimate bearing capacity of rock-socketed piles. Neural Comput Appl 2017;28:391–405.

[39] Momeni E, Armaghani DJ, Fatemi SA, Nazir R. Prediction of bearing capacity of thin-walled foundation: a simulation approach. Eng Comput 2018;34:319–27.

[40] Kulkarni RU, Dewaikar DM. Prediction of Interpreted Failure Loads of Rock-Socketed Piles in Mumbai Region using Hybrid Artificial Neural Networks with Genetic Algorithm. Int J Eng Res 2017;6:365–72.